







EVALUATION OF FERROCENYLMETHYLNUCLEOBASES DERIVATIVES INTERACTING WITH DNA: INSIGHTS FROM ELECTROCHEMICAL, SPECTROSCOPIC, DFT CALCULATION, MOLECULAR DOCKING AND MOLECULAR DYNAMIC SIMULATIONS

Mohammed Larbi Ben AMOR^{a,b}, Elhafnaoui LANEZ^{a,c,*} ,
Yahia BEKKAR^a , Aicha ADAIKA^a , Touhami LANEZ^a ,
Kaouther NESBA^d , Lazhar BECHKI^{e,f} 

ABSTRACT. This study investigates the binding of ferrocenylmethyl nucleobase derivatives to DNA through electrostatic interactions, employing a combination of experimental and theoretical approaches to elucidate binding mechanisms and explore their potential for DNA targeting. UV–Vis spectroscopy and cyclic voltammetry (CV) were used to evaluate binding affinities and structural alterations in DNA. The derivatives exhibited DNA interactions, evidenced by negative formal potential shifts in CV data. Binding constants and free binding energies derived from docking simulations aligned well with UV–Vis and CV analyses. Additionally, voltammetric data provided insights into the binding site size. Molecular docking simulations confirmed the critical role of electrostatic interactions in the binding of FcMeCy, FcMeTh,

-
- ^a *University of El Oued, Faculty of exact Sciences, Department of Chemistry, VTRS Laboratory, B.P.789, 39000, El Oued, Algeria*
^b *University of El Oued, Faculty of Technology, Department of Process Engineering and Petrochemical, P.O. Box 789, El Oued 39000, Algeria*
^c *University of El Oued, Faculty of Biology, Department of Cellular and Molecular Biology, 39000, El Oued, Algeria*
^d *University of El Oued, Faculty of Arts and Languages, Department of English Language, 39000, El Oued, Algeria*
^e *Kasdi Merbah University, Faculty of Mathematics and Material Sciences, Department of Chemistry, 30000, Ouargla, Algeria*
^f *Kasdi Merbah University, VPRS Laboratory, Department of Chemistry, Faculty of Mathematics and Material Sciences, 30000 Ouargla, Algeria*
* *Correspondent author e-mail: yahia-bekkar@univ-eloued.dz*



and (FcMe)₂Ad to DNA. Molecular dynamics simulations further revealed the stability of DNA-ligand complexes, with RMSD and radius of gyration (Rg) analyses indicating compact and stable DNA structures, emphasizing the robustness of these interactions for therapeutic applications. Theoretical investigations, including geometry optimization, Mulliken charge distribution, molecular electrostatic potential (MEP) analysis, and HOMO-LUMO surface analysis using density functional theory (B3LYP/aug-cc-pVTZ/6-311++G(d,p)), offered deeper insights into structural properties, reactive sites, and chemical reactivity. These results provide a comprehensive understanding of the interaction mechanisms and potential applications of these derivatives.

Keywords: *Ferrocene Nucleobase, Molecular dynamic simulation, Molecular docking, DFT*

INTRODUCTION

DNA functions as a template for protein synthesis, and its interactions with pharmacological agents can modulate protein replication, offering potential therapeutic strategies for cancer treatment [1,2]. Small molecules, including organometallic compounds, interact with cellular DNA, inducing damage either through direct interaction or by inhibiting enzymes responsible for maintaining DNA integrity [3–5]. Organometallic compounds that target DNA non-specifically, like cisplatin, are widely recognized as potent and successful anticancer drugs [6]. Since the late 1970s, ferrocene derivatives have been developed and investigated for their anticancer properties [7–11]. These derivatives are considered promising candidates due to their unique electrochemical characteristics and their capacity for robust interactions with DNA. Their effectiveness as anticancer agents have been demonstrated in various cancer cell lines, including those associated with breast cancer [12,13]. Over the past decade, significant research has focused on the chemistry of metal compounds and their interactions with DNA, aiming to enhance our understanding of their biological properties [14,15]. A number of these compounds have shown considerable biological activity when compared to standard pharmaceuticals [16–18].

Grasping the intricacies of the binding mechanisms and the variables that impact the affinity of these compounds for DNA is vital for creating and advancing effective agents that target DNA. This research aims to investigate the electrostatic binding interactions of N1-ferrocenylmethylcytosine (FcMeCy), N1-ferrocenylmethylthymine (FcMeTh), and N6,9-bis(ferrocenylmethyl)adenine ((FcMe)₂Ad) with chicken blood DNA (CB-DNA) through an integrated approach involving both theoretical and experimental methods. Techniques such as

UV–Vis spectroscopy and cyclic voltammetry (CV), alongside theoretical approaches including molecular docking, molecular dynamics simulations (MDS), and density functional theory (DFT), were employed to clarify the binding mechanisms and assess the capacity of these derivatives as DNA-targeting agents.

The findings demonstrate that all three compounds display a binding affinity for double-helical DNA via electrostatic interactions. Detailed insights into the free binding energies, binding constants, and binding site sizes were obtained from both theoretical and experimental data. This study enhances our knowledge of the electrostatic interactions between DNA and ferrocenylmethyl nucleobase derivatives, providing a foundation for their potential applications in DNA sensing and drug design.

RESULTS AND DISCUSSIONS

1. Cyclic Voltametric Studies

Figure S1 presents the cyclic voltametric response of 1 mM FcNB derivatives, both in the absence of and with progressively higher concentrations of CB-DNA at a bare glassy carbon electrode. The introduction of CB-DNA into the FcNB derivative solutions induced a negative shift in the anodic peak potential, along with a notable reduction in the anodic peak current density. This reduction is attributed to the formation of slowly diffusing adducts [19], which reduce the concentration of free compounds available for charge transfer reactions [20]. The observed negative shift is ascribed to the physical interaction between the FcNB derivatives and CB-DNA [21,22].

Binding constants (K_b) for the studied compounds were determined using **Equation 1**, which correlates the reduction in the anodic peak current density of the formed adducts to the free FcNB derivatives. In this equation, [DNA] is the DNA concentration, i_0 denotes the anodic peak current density in the absence of DNA and i indicates the anodic peak current density in the presence of DNA.

$$\log \frac{1}{[BSA]} = \log \frac{i}{i_0 - i} + \log K_b \quad (\text{Eq.1})$$

The binding number was determined to be 1, signifying the establishment of a 1:1 association complex between CB-DNA and the inclusion complexes [23]. K_b values for FcMeCy, FcMeTh, and (FcMe)₂Ad with CB-DNA were derived from the y-intercept of the linear plot of $\log(i/(i_0-i))$ versus $\log(1/[DNA])$ (**Figure S2**) and were calculated to be 3.25×10^4 , 4.75×10^4 , and $4.43 \times 10^4 \text{ M}^{-1}$, respectively.

The binding energies (ΔG in $\text{kJ}\cdot\text{mol}^{-1}$), as listed in **Table 1**, were calculated using **Equation 2** [11]:

$$\Delta G = -RT \ln K_b \quad (\text{Eq.2})$$

where T represents the absolute temperature equal to 301 K; R is the gas constant, $8.32 \text{ J}\cdot\text{mol}^{-1}\cdot\text{K}^{-1}$.

Table 1. The linear equations of $\log(i/(i_0-i))$ versus $\log(1/[\text{DNA}])$, binding free energy and binding constant values of FcMeCy-DNA, FcMeTh-DNA, and $(\text{FcMe})_2\text{Ad}$ -DNA obtained from CV data at pH = 7.2 and T = 301 K

Adduct	Equation	R ²	K _b (M ⁻¹)	-ΔG (kJ.mol ⁻¹)
FcMeCy-DNA	y = 0.839x + 4.511	0.992	3.25 × 10 ⁴	25.755
FcMeTh-DNA	y = 0.749x + 4.677	0.967	4.75 × 10 ⁴	26.701
(FcMe) ₂ Ad-DNA	y = 0.773x + 4.646	0.947	4.43 × 10 ⁴	26.528

1.1. Ratio of binding constants

The cyclic voltammograms shown in **Figure S3** illustrate the behavior of 1 mM solutions of FcMeCy, FcMeTh, and $(\text{FcMe})_2\text{Ad}$ in the absence and presence of 30 μM CB-DNA. These voltammograms facilitate the calculation of the binding constant ratios between the reduced form of the FcNB derivatives and CB-DNA, as well as the oxidized form $[\text{FcNB}]^+$ and CB-DNA. By examining the shifts in cathodic and anodic peak potentials caused by the introduction of CB-DNA, the binding constant ratios can be deduced [24].

When the presence of DNA induces shifts in both cathodic and anodic peak potentials, the equilibria depicted in **Figure S4** can be employed [25]. **Equation 3** is derived using the Nernst equation applied to these equilibria, describing the redox interactions of the studied compounds with DNA as shown in **Figure S3**.

$$\Delta E^0 = E_f^0 - E_b^0 = E^0(\text{FcNB}) - E^0(\text{FcNB} - \text{DNA}) = 0.06 \log \frac{K_{ox}}{K_{red}} \quad (\text{Eq.3})$$

In **Equation 3**, E_0^f and E_0^b represent the formal potentials of the $\text{FcNB}^+/\text{FcNB}$ redox pair for the free and DNA-bound states, respectively. The formal potential shifts, derived from the voltammograms in **Figure S3**, are summarized in **Table 2**. The binding constant ratios were determined using **Equation 3**, incorporating ΔE^0 values from **Table 2**. These binding constant ratios, also displayed in **Table 2**, indicate that the oxidized forms of the derivatives exhibit a slightly stronger binding affinity to DNA compared to their reduced forms.

Table 2. Electrochemical data of the free and DNA-bound FcMeCy, FcMeTh, and (FcMe)₂Ad used to calculate the ratio of the binding constants

Sample code	E _{pa}	E _{pc}	E ⁰ (V)	ΔE ⁰ (V)	K _{ox} /K _{red}
FcMeCy	0.2783	0.1991	0.2387	0.0219	2.351
FcMeCy-DNA	0.2567	0.1769	0.2168		
FcMeTh	0.4708	0.3569	0.41385	0.0624	11.397
FcMeTh-DNA	0.4026	0.3004	0.3515		
(FcMe) ₂ Ad	0.5436	0.4377	0.49065	0.0626	11.508
(FcMe) ₂ Ad-DNA	0.4815	0.3746	0.42805		

1.2. Diffusion coefficients

Figure S5 illustrates the electrochemical behavior of FcMeCy, FcMeTh, and (FcMe)₂Ad at varying scan rates, revealing distinct and stable anodic peaks. The diffusion coefficients of the free and DNA-bound forms of these compounds were calculated using the Randles–Sevcik **Equation 4** [26]:

$$i = 2.69 \times 10^5 n^3/2 S C D^{1/2} \nu^{1/2} \quad (\text{Eq.4})$$

where *i* represents the peak current (A), *n* is the number of electrons transferred during oxidation, *ν* is the scan rate (V.s⁻¹), *D* is the diffusion coefficient (cm².s⁻¹), *C* is the bulk concentration (mol cm⁻³) of the electroactive species, and *S* is the electrode surface area (cm²).

The linear relationship between the square root of the scan rates and the anodic peak current density (**Figure S6**) indicates a diffusion-controlled redox process [27]. Diffusion coefficients for both the free and DNA-bound ligands were derived from the slopes of the linear regressions based on **Equation 6**. The lower diffusion coefficients observed for the DNA-bound ligands compared to the free ligands further support the formation of adducts [28] (**Table 3**).

Table 3. Diffusion constants values of the free and DNA-bound forms of FcMeCy, FcMeTh, and (FcMe)₂Ad

Adduct	Equation	R ²	D (cm ² .s ⁻¹)
FcMeCy	y = 1.369x + 1.083	0.999	3.837 × 10 ⁻⁸
FcMeCy-DNA	y = 1.083x + 2.239	0.999	2.396 × 10 ⁻⁸
FcMeTh	y = 1.312x + 0.979	0.994	3.519 × 10 ⁻⁸
FcMeTh-DNA	y = 0.591x + 0.069	0.977	7.135 × 10 ⁻⁹
(FcMe) ₂ Ad	y = 1.801x + 1.174	0.996	6.631 × 10 ⁻⁸
(FcMe) ₂ Ad-DNA	y = 1.205x + 1.359	0.987	2.966 × 10 ⁻⁸

1.3. Binding site size

The binding site size (*s*) was determined using **Equation 5** [29]:

$$\frac{c_b}{c_f} = K \left[\frac{\text{free base pairs}}{s} \right] \quad (\text{Eq.5})$$

where C_b represents the concentration of ligand-DNA bound species, C_f is the concentration of free species, K is the binding constant, and s represents the binding site size in terms of base pairs.

Taking into account the concentration of DNA in terms of nucleotide phosphate [NP], the concentration of DNA base pairs can be expressed as $([DNA]/2)$. Consequently, **Equation 5** can be reformulated as:

$$\frac{C_b}{C_f} = K \frac{[DNA]}{2s} \quad (\text{Eq.6})$$

The ratio C_b/C_f can be expressed as $(i_0 - i)/i$ [30], where i_0 and i denote the experimental peak current densities in the absence and presence of DNA, respectively. The plots of C_b/C_f versus [DNA] are depicted in **Figure S7**.

The equations derived from the linear regression analysis for FcMeCy, FcMeTh, and $(FcMe)_2Ad$ within the investigated concentration range are shown in **Table 4**, where y represents the C_b/C_f ratio and x denotes the sample concentration, expressed in μM . The small values of the binding site size further imply an electrostatic interaction between FcMeCy, FcMeTh, and $(FcMe)_2Ad$ with DNA.

Table 4. Site size values of FcMeCy, FcMeTh, and $(FcMe)_2Ad$ obtained using the Plot of C_b/C_f versus [DNA]

Adduct	Equation	R ²	s
FcMeCy-DNA	$y = 0.031x - 0.034$	0.984	0.54092
FcMeTh-DNA	$y = 0.048x - 0.089$	0.895	0.49878
$(FcMe)_2Ad$ -DNA	$y = 0.043x - 0.071$	0.950	0.51428

2. Absorption spectral study

To corroborate the findings from the voltammetry experiments, the interaction between FcNB derivatives with CB-DNA was further investigated using electronic spectroscopy (ES) titration. This method enabled the evaluation of the interaction parameters of the FcNB-DNA complexes. As depicted in **Figure S8**, the absorption spectra for a constant concentration of each FcNB derivative were recorded, both without and with increasing amounts of CB-DNA.

The absorption bands at 435.4, 436.8, and 388.6 nm for all compounds displayed a reduction in intensity (hypochromicity) as the concentration of CB-DNA increased, without any significant hypsochromic shift. This clearly indicates the formation of the FcNB-DNA adducts [31,32]. The observed hypochromicity further supports the hypothesis that the primary interaction between FcNB derivatives and double-stranded CB-DNA is predominantly electrostatic [32,33].

The binding constants of the FcNB-DNA adducts were determined using the Benesi-Hildebrand **Equation 7**, which is founded on the reduction in

absorbance noted when FcNB compounds are added to a CB-DNA solution [33,34]:

$$\frac{A_0}{A-A_0} = \frac{\varepsilon_0}{\varepsilon-\varepsilon_0} \left(1 + \frac{1}{K_b[DNA]}\right) \quad (\text{Eq.7})$$

where A_0 and A denote the absorbance of the FcNB without and with CB-DNA, respectively, ε_0 and ε are their corresponding extinction coefficients. $[DNA]$ refers to the concentration of CB-DNA, and K_b denotes the binding constant. The plots of $1/[DNA]$ vs. $A_0/(A - A_0)$ are shown in **Figure S9**.

The linear correlation coefficients in the range of 0.993–0.998 suggest a binding stoichiometry of 1:1, indicating the formation of a 1:1 association adduct between the compounds and CB-DNA [35].

The binding constants of FcNB derivatives with CB-DNA were determined by calculating the ratio of the slope to the y-intercept of the linear equation, which allowed for the derivation of binding free energies. The values obtained for FcMeCy, FcMeTh, and (FcMe)₂Ad were -24.73, -24.78, and -25.20 kJ·mol⁻¹, respectively, as presented in **Table 5**. Both spectroscopic and electrochemical analyses indicate that all FcNB derivatives can form relatively stable inclusion complexes with CB-DNA.

Table 5. The linear equations of $1/[DNA]$ versus $A_0/(A-A_0)$, binding free energy and binding constant values of FcMeCy-DNA, FcMeTh-DNA, and (FcMe)₂Ad-DNA obtained from ES data at pH = 7.2 and T = 301 K

Adduct	Equation	R ²	K _b (M ⁻¹)	-ΔG (kJ·mol ⁻¹)
FcMeCy-DNA	y = -168.768x + 3.629	0.998	2.15 × 10 ⁴	24.73
FcMeTh-DNA	y = -465.596x + 10.213	0.993	2.19 × 10 ⁴	24.78
(FcMe) ₂ Ad-DNA	y = -689.716x + 17.905	0.997	2.59 × 10 ⁴	25.20

3. Viscosity measurement

Viscosity studies complement spectroscopic methods by providing precise insights into the interaction mechanisms of small molecules with DNA [36,37]. This straightforward and highly sensitive technique can detect changes in DNA length induced by such interactions [38]. In this research, viscosity measurements were conducted to elucidate the binding modes of FcMeCy, FcMeTh, and (FcMe)₂Ad with CB-DNA. Classical intercalators like ethidium bromide (EB) typically cause a substantial increase in DNA viscosity. This effect is due to the extension of the DNA molecule as base pairs are separated at the intercalation sites, leading to an overall increase in DNA length. In contrast, interactions through electrostatic or groove binding do not alter the DNA length significantly, thus exhibiting minimal or no effect on DNA viscosity [39].

Figure 1 shows the influence of increasing concentrations of FcMeCy, FcMeTh, (FcMe)₂Ad, and EB on the viscosity of CB-DNA. The results

indicate that higher concentrations of FcMeCy, FcMeTh, and (FcMe)₂Ad do not significantly alter CB-DNA viscosity, corroborating the conclusion that these compounds bind to CB-DNA primarily through electrostatic or groove binding modes. These conclusions are further supported by the UV-Vis spectroscopy data.

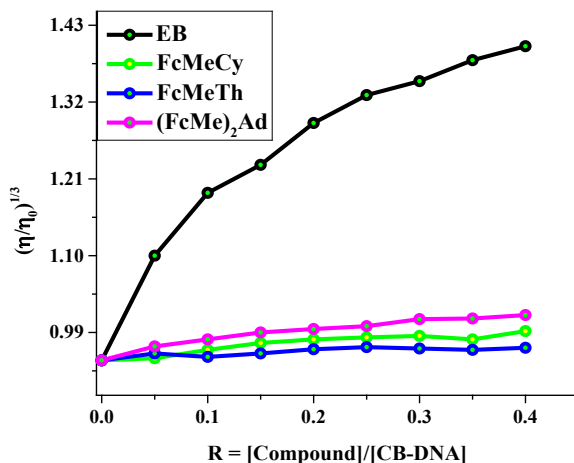


Figure 1. The effect of various concentrations of FcMeCy, FcMeTh, (FcMe)₂Ad, and EB on the viscosity of CB-DNA.

4. Theoretical approach

4.1. Structure optimization

Optimizing the structure of small molecules is essential for accurately determining their binding behavior. To elucidate this, the structures of FcMeCy, FcMeTh, and (FcMe)₂Ad were fully optimized using the DFT/B3LYP method, as detailed in the Materials and Methods Section. The optimized geometries of these compounds are depicted in **Figure S10**. This figure shows that the ferrocene portion of these molecules features a sandwich-like structure, consisting of two cyclopentadienyl rings with an Fe²⁺ ion positioned between them. As illustrated in **Figure S10**, the optimized geometry of FcMeCy and FcMeTh align well with their X-ray crystallographic structure.

4.2. MEP surface and atomic charge

The molecular electrostatic potential (MEP) surface visualizes charge distribution, identifying electron-rich (red, electrophilic sites) and electron-deficient (blue, nucleophilic sites) regions [40,41]. **Figure S11** presents the MEP maps for FcMeCy, FcMeTh, and (FcMe)₂Ad. In all cases, oxygen and

nitrogen atoms of the nucleobases exhibit negative electrostatic potential, highlighting their susceptibility to electrophilic interactions, while the ferrocene moiety remains electrostatically neutral. The MEP values range from $-2.375 \cdot 10^{-2}$ to $+2.375 \cdot 10^{-2}$ for FcMeCy, $-1.747 \cdot 10^{-2}$ to $+1.747 \cdot 10^{-2}$ for FcMeTh, and $-0.90 \cdot 10^{-2}$ to $+0.90 \cdot 10^{-2}$ for (FcMe)₂Ad.

Mulliken charge analysis further supports these findings, indicating that oxygen atoms carry negative charges, reinforcing their role in potential electrophilic interactions. The dipole moments calculated for FcMeCy, FcMeTh, and (FcMe)₂Ad were 5.773, 5.091, and 2.652 Debye, respectively.

4.3. HOMO-LUMO analysis

The HOMO-LUMO energy gap (ΔE_{L-H}) provides insights into molecular stability and reactivity [42,43]. **Figure S12** presents the HOMO-LUMO surfaces for FcMeCy, FcMeTh, and (FcMe)₂Ad, showing HOMO localization on the ferrocene moiety and LUMO association with the nucleobase group. The calculated energy gaps are 4.338 eV (FcMeCy), 4.397 eV (FcMeTh), and 4.496 eV ((FcMe)₂Ad), indicating an increasing stability trend: (FcMe)₂Ad > FcMeTh > FcMeCy. Correspondingly, chemical reactivity follows the reverse order: FcMeCy > FcMeTh > (FcMe)₂Ad.

Additional quantum descriptors (**Table 6**) reveal that FcMeTh exhibits the highest electrophilicity index ($\omega = 3.02$), indicating a greater tendency to interact with biomolecules such as DNA. The absolute electronegativity (χ) suggests that FcMeTh is the strongest Lewis acid among the three compounds. Lower chemical hardness (η) and higher softness (σ) for FcMeCy and FcMeTh indicate greater reactivity compared to (FcMe)₂Ad. These results suggest FcMeTh's strong potential for biomolecular interactions due to its higher electrophilicity and lower chemical hardness.

Table 6. The calculated quantum chemical parameter for FcMeCy, FcMeTh, and (FcMe)₂Ad using DFT

Compound	FcMeCy	FcMeTh	(FcMe) ₂ Ad
E_{HOMO}	-5.577	-5.840	-5.431
E_{LUMO}	-1.189	-1.443	-0.935
ΔE_{L-H}	4.338	4.397	4.496
χ	3.38	3.64	3.18
Π	-3.38	-3.64	-3.18
η	2.19	2.20	2.25
σ	0.46	0.45	0.44
ω	2.61	3.02	2.25
ΔN_{max}	1.54	1.66	1.42

5. Molecular docking evaluation

Molecular docking simulations are an essential tool for elucidating the interactions between small molecules and DNA at an atomic level, playing a critical role in the process of drug discovery. These simulations provide insights into the DNA-drug interaction mechanisms, thereby aiding rational drug design [44]. In this investigation, the binding sites of DNA with the compounds FcMeCy, FcMeTh, and (FcMe)₂Ad were examined to validate our experimental results and predict the interaction types within the DNA-compound system [45]. The simulations identify the most stable binding poses ($\Delta G < 0$) of these compounds when bound to a macromolecule.

Multiple docking runs were executed, revealing that the most favorable binding energies for FcMeCy, FcMeTh, and (FcMe)₂Ad with DNA were -6.77, -6.59, and -7.60 Kcal/mol, respectively. This indicates a robust interaction between DNA and (FcMe)₂Ad, following the binding strength order: (FcMe)₂Ad > FcMeCy > FcMeTh. These findings are consistent with those obtained from electronic absorption spectroscopy. As shown in **Figure S13**, FcMeCy, FcMeTh, and (FcMe)₂Ad engage with DNA through a groove binding mode, primarily facilitated by electrostatic interactions.

For FcMeCy, the interaction with DNA is characterized by: (i) a strong electrostatic attraction between the aniline group and DC9 (Electrostatic Attraction Distance, EAD = 1.911 Å), and (ii) two hydrogen bonds between DG10 and the carbonyl group (=O) (Hydrogen Bond Distances, HBD = 2.075 Å and 2.1 Å). The interaction of FcMeTh with DNA involves two hydrogen bonds between DG10 and the carbonyl group (HBD = 2.018 Å and 1.859 Å). For (FcMe)₂Ad, the interactions include: (i) a strong electrostatic attraction between DC21 and the aniline group (EAD = 1.874 Å), and (ii) a hydrogen bond between DA5 and a nitrogen atom (HBD = 2.024 Å). These interactions suggest that FcMeCy forms more extensive interactions with DNA compared to FcMeTh and (FcMe)₂Ad, which is in agreement with the global electrophilicity (ω) values. Consequently, electrostatic interactions are crucial for the binding of FcMeCy, FcMeTh, and (FcMe)₂Ad to DNA. The docking simulation results align well with those from UV-Vis and viscosity experiments, though minor discrepancies in ΔG values are attributed to the computational studies being conducted in the vacuum, while experimental measurements were performed in the solid phase [46].

6. Molecular dynamic simulation

6.1. Root mean square deviation (RMSD)

Molecular dynamics (MD) simulations were performed to evaluate the stability of the DNA-ligand complexes [47]. The optimal binding poses obtained from the docking studies served as the initial configurations for these

simulations. To examine systematic deviations over time, the root mean square deviation (RMSD) values for all complexes were calculated and plotted, as depicted in **Figure 2**.

The analysis of RMSD profiles reveals interesting stability patterns for the DNA-ligand complexes under study. FcMeCy and FcMeTh consistently maintain their binding to DNA, as indicated by their RMSD values, which remain below 2.5 Å throughout the simulation duration. This minimal deviation from the initial structure signifies a stable interaction, with the convergence of RMSD values further underscoring the robustness of these complexes (**Figure 2**). In stark contrast, the (FcMe)₂Ad complex demonstrates significant instability, with RMSD values showing significant fluctuations, reaching up to 9.78 Å over the 100 ns simulation period. This pronounced deviation highlights a lack of structural stability, suggesting that the (FcMe)₂Ad complex does not maintain a consistent binding configuration with DNA.

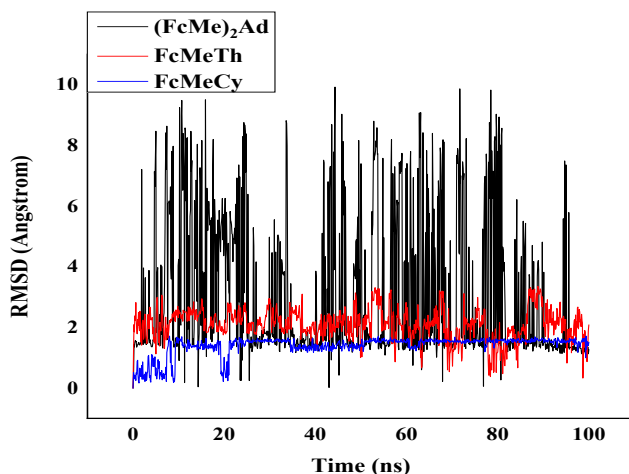


Figure 2. RMSD graphs for: FcMeCy, FcMeTh, and (FcMe)₂Ad ligands complexed with DNA during 100 ns.

6.2. Radius of gyration (Rg)

To assess the structural compactness of DNA when bound to FcMeCy, FcMeTh, and (FcMe)₂Ad, we analyzed the radius of gyration (Rg). This metric provides insights into DNA compactness, where lower Rg values indicate tighter packing, while higher values suggest potential unfolding during the simulations [48]. Throughout the simulation period, the Rg values for FcMeCy and FcMeTh complexes remained stable, ranging from 2.17 to 3.75 Å, as shown in **Figure 3**.

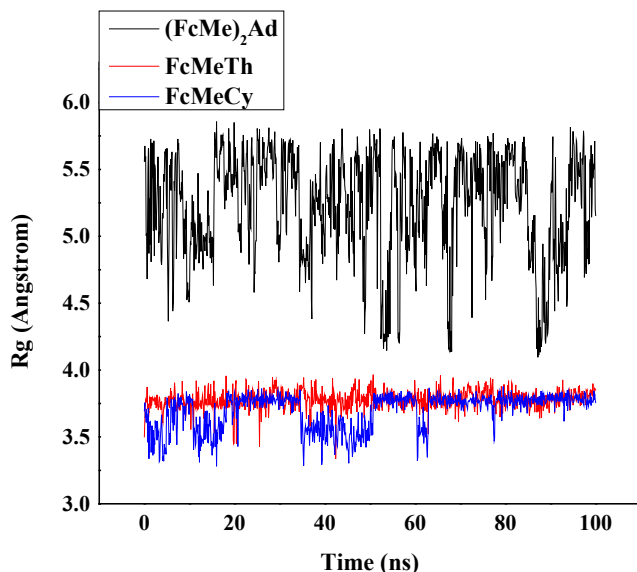


Figure 3. The Rg plots of FcMeCy, FcMeTh, and (FcMe)₂Ad complexes as a function of simulation time

This stability indicates that DNA maintains a compact conformation when interacting with these compounds. The consistent Rg values align with the RMSD results, further confirming the structural robustness of these complexes. However, the (FcMe)₂Ad complex displayed significantly higher Rg values, between 4.39 and 5.69 Å, throughout the simulation. This indicates a less compact structure and suggests that (FcMe)₂Ad induces structural changes, leading to potential unfolding or destabilization of the DNA. The elevated Rg values correspond with the higher RMSD values observed for (FcMe)₂Ad, highlighting its relative instability compared to the other two compounds.

MATERIALS AND MEASUREMENTS

1. Chemical and Reagents

Reagents and solvents used in this study were of analytical grade and sourced from various commercial suppliers, with no additional purification performed. Chicken blood samples were collected from a butcher in Eloued city using sterilized 20 ml bottles containing 2 ml of EDTA [49]. These samples were stored at 0°C and were processed for extraction within 24

hours [50]. All stock solutions were freshly prepared and utilized within five days, stored at 4 °C until needed. The phosphate buffer solution (PBS), maintaining a physiological pH of 7.2, was prepared with disodium hydrogen phosphate and sodium dihydrogen phosphate from Sigma-Aldrich, along with double-distilled water. Tetrabutylammonium tetrafluoroborate (Bu_4NBF_4) (electrochemical grade 99%; Sigma-Aldrich) served as the supporting electrolyte. Nitrogen gas, used in the experiments, was supplied from a research-grade cylinder (99.99%; Linde Gaz Algeria). All results presented in this study reflect the average of three independent experimental measurements.

2. Synthesis

N1-ferrocenylmethylcytosine (FcMeCy), N1-ferrocenylmethylthymine (FcMeTh) and N6,9-bis(ferrocenylmethyl)adenine ((FcMe) $_2$ Ad) synthesized through the reaction of the quaternary salt N,N,N-trimethylammonium-methylferrocene iodide with cytosine, thymine and adenine, respectively, following the procedure previously reported by our group [51,52]. The analytical and spectroscopic data obtained for all compounds were consistent with the proposed structures (Figure 4).

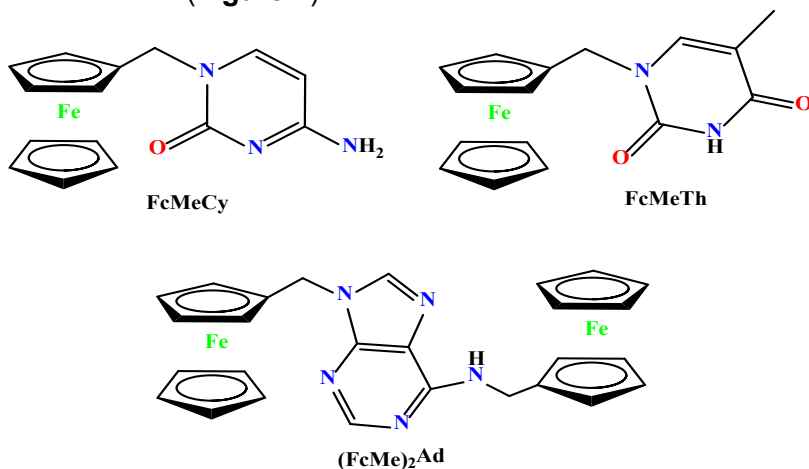


Figure 4. Structures of FcMeCy, FcMeTh, FcMeAd and (FcMe) $_2$ Ad

3. DNA Extraction

DNA was extracted from chicken blood (CB-DNA) using established protocols [53,54]. After extraction, the DNA was dissolved in a PBS at pH 7.2, diluted with 90% aqueous ethanol, and subsequently stored at 4 °C. The concentration of the DNA stock solution was determined by measuring UV absorbance at 260 nm, using a molar absorption coefficient of $6600 \text{ M}^{-1} \text{ cm}^{-1}$ [55].

The purity of the extracted DNA was verified by the absorbance ratio at 260 nm and 280 nm, which was ranged from 1.69 to 1.90, indicating minimal protein contamination [56].

To prepare 10 mM stock solutions of the compounds, each compound was accurately weighed and dissolved in 5 mL of distilled water. The solutions were buffered with a PBS (0.1 M $\text{KH}_2\text{PO}_4/\text{K}_2\text{HPO}_4$) to maintain a pH of 7.2. This buffering condition was chosen to avoid the degradation of the ferrocenium state in basic environments and to prevent the protonation of the ferrocenyl group in highly acidic conditions [57].

4. Cyclic Voltammetry Measurements

Cyclic voltammetry experiments were performed using a VoltaLab 40 (Radiometer Analytical SAS, France) linked to an electrochemical cell. This cell featured a glassy carbon electrode (area: 0.077 cm^2) as the working electrode, and a 0.5 mm thick platinum wire as the counter electrode a saturated calomel electrode as the reference electrode. Voltammograms were recorded for each compound solution, both in the absence and presence of various concentrations of CB-DNA. Prior to measurements, the solutions were purged with nitrogen gas for 15 minutes to eliminate dissolved oxygen. Between each electrochemical assay, the working electrode was meticulously cleaned and polished.

5. UV-Vis Spectroscopic Measurements

Absorption spectra were recorded using a Shimadzu 1800 UV-Vis spectrometer (Japan). Initially, the electronic spectra of 1 mM FcMeCy, FcMeTh and $(\text{FcMe})_2\text{Ad}$ were measured in a 0.1 M PBS at pH 7.2 and a temperature of 298 K. Subsequently, the spectral responses were assessed by adding gradually increasing concentrations of CB-DNA solution to the solution samples. Each sample was allowed to stabilize for at least 5 minutes before each measurement.

6. Viscosity Measurement

To corroborate the findings from absorption spectroscopy, interactions with DNA were further investigated through detailed hydrodynamic studies, specifically viscosity measurements. These investigations involved altering the concentration of the compounds while keeping the DNA concentration constant, utilizing an Ostwald viscometer. The experiments were conducted in triplicate, and the average flow time was determined using a digital stopwatch. Ethidium bromide (EB), a standard intercalator, was used as a control. The concentrations of ferrocenylmethyl nucleobase (FcNB) derivatives and EB

were varied from 0 to 24 μM , while the concentration of CB-DNA was kept constant at 0.1 mM to achieve binding ratios (R) ranging from 0.00 to 0.40 ($R = [\text{compounds}]/[\text{CB-DNA}]$). Viscosity measurements were calculated using **Equation 8**. [58,59].

$$\eta = \frac{(t-t^0)}{t^0} \quad (\text{Eq.8})$$

While t^0 represents the flow time of the pure compound and t denotes the flow time of the compound-DNA solution, where η is the viscosity of the solution. The results were plotted as $(\frac{\eta}{\eta_0})^{1/3}$ against the binding ratio R [60].

7. DFT calculation

Utilizing the density functional theory (DFT) methodology, the geometry optimization of FcNB derivatives was performed with Gauss View 6.0 for visualization and the Gaussian 09 W package [61,62]. The compounds were fully optimized using the B3LYP correlation functional, employing the aug-cc-pVTZ basis set for the iron (Fe) atom and the 6-311++G(d,p) basis set for lighter atoms such as carbon (C), hydrogen (H), nitrogen (N), and oxygen (O) [63]. All calculations were conducted in the gas phase at the ground state to determine the intrinsic electronic properties of the compounds. While DFT calculations in vacuum do not fully capture biological environments, they provide a reliable foundation for understanding fundamental electronic properties, charge distributions, and molecular reactivity. These insights serve as a basis for further computational and experimental investigations in solution-phase or biological contexts. Additionally, the study encompassed an examination of molecular electrostatic potential (MEP) surfaces, Mulliken charge distribution, and frontier molecular orbitals (FMOs) including HOMO (highest occupied molecular orbital) and LUMO (lowest unoccupied molecular orbital) surfaces. These analyses were aimed at identifying electrophilic and nucleophilic regions as well as assessing the reactivity of the compounds, all conducted under the same theoretical framework.

8. Molecular docking

8.1. Receptor preparation

A DNA segment (PDB ID: 453D) was selected for docking experiments, with its X-ray crystal structure (resolution: 1.80 Å; R-value: 0.251) obtained from the RCSB Protein Data Bank [64]. This DNA structure, which comprises the sequence 5'-D(*CP*GP*CP*GP*AP*AP*TP*TP*CP*G-P*CP*G)-3', was

originally complexed with benzimidazole. To prepare the DNA segment for docking studies, benzimidazole and all water molecules were eliminated from the protein using AutoDock Tools 1.5.6 (ADT) software [65]. Although DNA in solution exhibits dynamic flexibility, the selected structure provides a reasonable approximation for studying molecular interactions, as supported by previous studies [66–69].

8.2. Structural optimization

The 3-dimensional structures of the ligands were constructed initially, and the most stable conformer of each was identified using Spartan software [70] with the semiempirical PM6 method [71]. Subsequently, the optimal conformer for each ligand was refined using density functional theory (DFT) with the B3LYP/6-311++G(d,p) method, which includes dispersion interactions [72], implemented in Gaussian software. This approach was selected based on prior benchmark studies of ferrocene derivatives conducted by our research group [49,50]. The optimized structures of all ligands were saved in pdb format. All iron atoms coordinated within the ferrocene moiety in this study were maintained in the +1-oxidation state.

8.3. Docking simulations

The ADT software [65] was utilized to prepare docking input files for each ferrocene derivatives structure and the DNA segment. Hydrogen atoms were added to the crystal structure. A grid box measuring 80, 80, and 100 points along the x, y, and z axes, respectively, was centered on the DNA to encompass the entire structure. Each docking process was set to generate 10 poses, following default parameters. Docking simulations were performed using AutoDock Vina, which provided binding affinities represented as Gibbs free binding energies. Previous studies have successfully employed similar methodologies to investigate ferrocene interactions with biomolecules, yielding meaningful insights [66–69]. The structure with the most favorable binding free energy was selected and further analyzed using Discovery Studio 4.5 [73]. In the scoring process, metals are treated as hydrogen bond donors, potentially affecting the differentiation of substrates with different metal compositions [74,75].

The binding free energies (ΔG in kcal/mol) obtained from AutoDock Vina were subsequently used to calculate binding constants (K_b) using **Equation 9**:

$$K_b = e^{[(\Delta G \times 1000)/RT]} \quad (\text{Eq.9})$$

where R represents the universal gas constant (1.987 cal/mol.K), and T is the temperature (298 K).

9. Molecular dynamics simulation

Molecular dynamics (MD) simulations were conducted using the Desmond simulation software from Schrödinger LLC [76]. All simulations utilized the NPT ensemble at a temperature of 300 K and a pressure of 1 bar. Each simulation was conducted for duration of 100 ns, with a relaxation time of 1 ps for all ligands. The OPLS force field parameters were consistently applied throughout the simulations. [77]. Long-range electrostatic interactions were computed using the particle mesh Ewald method [78], employing a Coulomb interaction cutoff radius of 9.0 Å. Water molecules were modelled using the simple point charge model [79]. Implicit solvent effects were considered to partially account for ionic interactions. Pressure control employed the Martyna-Tuckerman-Klein chain coupling scheme [80] with a coupling constant of 2.0 ps, while temperature control utilized the Nose-Hoover chain coupling scheme [80]. Nonbonded forces were computed using an r-RESPA integrator, updating short-range forces every step and long-range forces every three steps. Trajectories were saved every 4.8 ps for subsequent analysis.

The Desmond MD package's Simulation Interaction Diagram tool was utilized to investigate the interactions between ligands and DNA. The stability of MD simulations was assessed by monitoring the Root Mean Square Deviation (RMSD) of ligand atoms over time. This analysis focused on the DNA-ligand complexes involving FcMeCy, FcMeTh and ((FcMe)₂Ad, with detailed findings presented in the Results and Discussion section.

CONCLUSION

In this study, we explored how ferrocenylmethyl nucleobase derivatives (FcMeCy, FcMeTh, and (FcMe)₂Ad) interact with DNA through both experimental and theoretical methods. Our findings showed strong electrostatic interactions and binding affinity, highlighted by a noticeable negative shift in the anodic peak potential during cyclic voltammetry. The DFT analyses confirmed that bond lengths and angles were consistent, while the MEP analysis pointed out that the nucleobase groups are particularly susceptible to nucleophilic attack. From the HOMO-LUMO analysis, we found that the energy gap follows this order: (FcMe)₂Ad > FcMeTh > FcMeCy. Docking studies underlined the importance of electrostatic interactions in the binding process, with the binding constants aligning well with our experimental data. In molecular dynamics simulations, FcMeCy and FcMeTh showed stable binding to DNA, as evidenced by RMSD values remaining below 1.5 Å

throughout the simulations, which indicates the formation of stable complexes. Additionally, the R_g measurements remained steady, suggesting that DNA's compactness was preserved even in the presence of these ligands. These results underscore the interactions between DNA and the ferrocenylmethyl derivatives and point to their potential for further exploration in therapeutic applications.

SUPPLEMENTARY INFORMATION

The supplementary data for this study, including additional computational details and supporting figures, have been deposited in Mendeley Data and are publicly accessible at:

BEN AMOR, Mohammed Larbi; LANEZ, Elhafnaoui; Bekkar, Yahia; ADAIKA, Aicha; LANEZ, Touhami; NESBA, Kaouther; BECHKI, Lazhar (2025), "Evaluation of Ferrocenylmethylnucleobases Derivatives Interacting with DNA: Insights from Electrochemical, Spectroscopic, DFT Calculation, Molecular Docking and Molecular Dynamic Simulations", Mendeley Data, V1, DOI: 10.17632/kht6hnrw4s.1.

CREDIT AUTHORSHIP CONTRIBUTION STATEMENT

M. L. BEN AMOR: Software, formal analysis, investigation, methodology, writing reviewing and editing. E. LANEZ: Supervision, validation, writing—reviewing and editing. Y. Bekkar: validation, writing, reviewing and editing. A. ADAIKA: Software, writing and editing. T. LANEZ: Supervision, validation. K. NESBA: writing and editing. L. BECHKI: Supervision, validation.

DECLARATION OF COMPETING INTEREST

The authors declare that they have no known competing financial interests or personal relationships that could have appeared to influence the work reported in this paper.

ACKNOWLEDGMENTS

This work was supported by the directorate-general of scientific research and technological development (DGRSDT) and the laboratory of valorization and technology of Saharan resources (VTRS) (project code: B00L01UN390120150001).

FUNDING DECLARATION

This research did not receive any specific grant from funding agencies in the public, commercial, or not-for-profit sectors.

REFERENCES

1. Y. Sun, Y. Liu, X. Ma, H. Hu, *Int J Mol Sci*, **2021**, *22*, 6923.
2. J.F. Alhmod, J.F. Woolley, A.-E. Al Moustafa, M.I. Mallei, **2021**, 309–339.
3. R. Mehandi, R. Arif, M. Rana, S. Ahmedi, R. Sultana, M.S. Khan, M. Maseet, M. Khanuja, N. Manzoor, N. Nishat, *J Mol Struct*, **2021**, 1245, 131248.
4. M. Rana, M.I. Faizan, S.H. Dar, T. Ahmad, Rahisuddin, *ACS Omega*, **2022**, *7*, 22639–22656.
5. E.J. Anthony, E.M. Bolitho, H.E. Bridgewater, O.W.L. Carter, J.M. Donnelly, C. Imberti, E.C. Lant, F. Lermite, R.J. Needham, M. Palau, *Chem Sci*, **2020**, *11*, 12888–12917.
6. J. Zegers, M. Peters, B. Albada, **2023**, *28*, 117–138.
7. Q. Cheng, T. Zhou, Q. Xia, X. Lu, H. Xu, M. Hu, S. Jing, *RSC Adv*, **2021**, *11*, 25477–25483.
8. L. Tabrizi, T.L.A. Nguyen, H.D.T. Tran, M.Q. Pham, D.Q. Dao, *J Chem Inf Model*, **2020**, *60*, 6185–6203.
9. C. Ornelas, **2011**, *35*, 1973–1985.
10. N. Zegheb, C. Boubekri, T. Lanez, E. Lanez, T.T. Küçükılınç, E. Öz, A. Khenoufa, S. Khamouli, S. Belaidi, *Anticancer Agents Med Chem*, **2021**, *22*, 1426–1437.
11. A. Khenoufa, L. Bechki, T. Lanez, E. Lanez, N. Zegheb, *J Mol Struct*, **2021**, 1224, 129052.
12. G. Gasser, I. Ott, N. Metzler-Nolte, *J Med Chem*, **2011**, *54*, 3–25.
13. R. Wang, H. Chen, W. Yan, M. Zheng, T. Zhang, Y. Zhang, *Eur J Med Chem*, **2020**, *190*, 112109.
14. A.M. Abu-Dief, M.A. Said, O. Elhady, N. Alahmadi, S. Alzahrani, T.N.A. Eskander, M.A.E.A.A. Ali, *Inorg Chem Commun*, **2023**, 155, 110955.
15. S. Masood, M. Jamshaid, M.N. Zafar, E.U. Mughal, M. Ashfaq, M.N. Tahir, *J Mol Struct*, **2024**, 1295, 136571.
16. M. Sumi, N.T. Nevaditha, B.S. Kumari, *J Mol Struct*, **2023**, 1272, 134091.
17. A.M. Abu-Dief, R.M. El-Khatib, T. El-Dabea, A. Abdou, F.S. Aljohani, E.S. Al-Farraj, I.O. Barnawi, M.A.E.A.A. Ali, *J Mol Liq*, **2023**, 386, 122353.
18. A.M. Abu-Dief, M.A. Said, O. Elhady, H.A. Al-Abdulkarim, S. Alzahrani, T.N.A. Eskander, M.A.E.A.A. El-Remaily, *Appl Organomet Chem*, **2023**, *37*, e7162.
19. M. Hanane, T. Lanez, I. Zafar, M.S. Afghan, N. Zegheb, *J Coord Chem*, **2023**, *76*, 1984–1998.
20. H. Mouada, T. Lanez, I. Zafar, *J Organomet Chem*, **2024**, 1007, 123026.
21. N. Li, Y. Ma, C. Yang, L. Guo, X. Yang, *Biophys Chem*, **2005**, *116*, 199–205.

22. M.T. Carter, M. Rodriguez, A.J. Bard, *J Am Chem Soc*, **1989**, 111, 8901–8911.
23. P. Şenel, S. Agar, M. Yurtsever, A. Gölcü, *J Pharm Biomed Anal*, **2023**, 115746.
24. A. Shah, M. Zaheer, R. Qureshi, Z. Akhter, M.F. Nazar, *Spectrochim Acta A Mol Biomol Spectrosc*, **2010**, 75, 1082–1087.
25. X. Chu, G.-L. Shen, J.-H. Jiang, T.-F. Kang, B. Xiong, R.-Q. Yu, *Anal Chim Acta*, **1998**, 373, 29–38.
26. C.M.A. Brett, O. Brett, **1993**, 67, 444.
27. E. Lanez, M. Saidi, T. Lanez, **2023**, 44, 542–558.
28. M.A. Neelakantan, F. Rusalraj, J. Dharmaraja, S. Johnsonraja, T. Jeyakumar, M. Sankaranarayana Pillai, *Spectrochim Acta A Mol Biomol Spectrosc*, **2008**, 71, 1599–1609.
29. G.-C. Zhao, J.-J. Zhu, J.-J. Zhang, H.-Y. Chen, *Anal Chim Acta*, **1999**, 394, 337–344.
30. M. Aslanoglu, G. Ayne, *Anal Bioanal Chem*, **2004**, 380, 658–663.
31. T. Sarwar, S.U. Rehman, M.A. Husain, H.M. Ishqi, M. Tabish, *Int J Biol Macromol*, **2015**, 73, 9–16.
32. D.K. Jangir, S. Charak, R. Mehrotra, S. Kundu, *J Photochem Photobiol B*, **2011**, 105, 143–148.
33. K. Roy, S. Kar, P. Ambure, **2015**, 145, 22–29.
34. N. Shahabadi, M. Falsafi, *Spectrochim Acta A Mol Biomol Spectrosc*, **2014**, 125, 154–159.
35. A.M. Abu-Dief, T. El-Dabea, R.M. El-Khatib, M. Feizi-Dehnayebi, F.S. Aljohani, K. Al-Ghamdi, I.O. Barnawi, M.A.E.A.A. Ali, *J Mol Liq*, **2024**, 399, 124422.
36. D. Suh, J.B. Chaires, *Bioorg Med Chem*, **1995**, 3, 723–728.
37. S.Z. Moradi, A. Nowroozi, K. Sadrjavadi, S. Moradi, K. Mansouri, L. Hosseinzadeh, M. Shahlaei, *Int J Biol Macromol*, **2018**, 114, 40–53.
38. F.A. Qais, K.M. Abdullah, M.M. Alam, I. Naseem, I. Ahmad, *Int J Biol Macromol*, **2017**, 97, 392–402.
39. Z. Seferoğlu, M.M.A. Mahmoud, H. Ihmels, **2016**, 125, 241–248.
40. M. Milusheva, M. Todorova, V. Gledacheva, I. Stefanova, M. Feizi-Dehnayebi, M. Pencheva, P. Nedialkov, Y. Tumbarski, V. Yanakieva, S. Tsoneva, **2023**, 16, 1660.
41. A.S. Dorafshan Tabatabai, E. Dehghanian, H. Mansouri-Torshizi, M. Feizi-Dehnayebi, *J Biomol Struct Dyn*, **2024**, 42, 5447–5469.
42. I.M. Khan, M. Islam, S. Shakya, N. Alam, S. Imtiaz, M.R. Islam, *J Biomol Struct Dyn*, **2022**, 40, 12194–12208.
43. S. Shakya, I.M. Khan, B. Shakya, Y.H. Siddique, H. Varshney, S. Jyoti, *J Mater Chem B*, **2023**, 11, 1262–1278.
44. I.M. Khan, S. Shakya, R. Akhtar, K. Alam, M. Islam, N. Alam, *Bioorg Chem*, **2020**, 100, 103872.
45. I.M. Khan, S. Shakya, M. Islam, S. Khan, H. Najnin, *Phys Chem Liquids*, **2021**, 59, 753–769.
46. M. Feizi-Dehnayebi, E. Dehghanian, H. Mansouri-Torshizi, *J Mol Struct*, **2021**, 1240, 130535.

47. H. Laraoui, E. Lanez, N. Zegheb, A. Adaika, T. Lanez, M. Benkhaled, *ChemistrySelect*, **2023**, 8, e202204512.
48. M.T. Rehman, M.F. AlAjmi, A. Hussain, *Curr Pharm Des*, **2021**, 27, 3577–3589.
49. T. Lanez, M. Feizi-Dehnayebi, E. Lanez, *J Mol Struct*, **2024**, 138386.
50. A. Yahiaoui, N. Benyza, A. Messai, T. Lanez, E. Lanez, **2023**,.
51. E. Lanez, L. Bechki, T. Lanez, **2019**, 20,.
52. E. Lanez, L. Bechki, T. Lanez, *Chemistry (Easton)*, **2020**, 14, 146–153.
53. E. Lanez, L. Bechki, T. Lanez, **2019**, 13, 11–17.
54. T. Lanez, H. Benaicha, E. Lanez, M. Saidi, **2018**, 39, 76–88.
55. R. Vijayalakshmi, M. Kanthimathi, V. Subramanian, B.U. Nair, *Biochem Biophys Res Commun*, **2000**, 271, 731–734.
56. J.A. Glasel, *Biotechniques*, **1995**, 18, 62–63.
57. C.-S. Lu, X.-M. Ren, C.-J. Hu, H.-Z. ZHU, Q.-J. MENG, *Chem Pharm Bull (Tokyo)*, **2001**, 49, 818–821.
58. R. Bera, B.K. Sahoo, K.S. Ghosh, S. Dasgupta, *Int J Biol Macromol*, **2008**, 42, 14–21.
59. S. Qamar, F. Perveen, Z. Akhter, S. Yousuf, M. Sultan, S.E. Ela, N. Ullah, M. Fatima, K. Fatima, U. Nazir, *J Mol Struct*, **2022**, 1253, 132250.
60. S. Satyanarayana, J.C. Dabrowiak, J.B. Chaires, *Biochemistry*, **1992**, 31, 9319–9324.
61. M. Frisch, F. Clemente, **2009**, 20–44.
62. R. Dennington, T.A. Keith, J.M. Millam, **2016**,.
63. N.B. Balabanov, K.A. Peterson, *J Chem Phys*, **2005**, 123,.
64. H.M. Berman, *Nucleic Acids Res*, **2000**, 28, 235–242.
65. G.M. Morris, R. Huey, W. Lindstrom, M.F. Sanner, R.K. Belew, D.S. Goodsell, A.J. Olson, *J Comput Chem*, **2009**, 30, 2785–2791.
66. E. Lanez, A. Kedadra, T. Lanez, A. Adaika, N. Zegheb, *J Organomet Chem*, **2024**, 1017, 123284.
67. A. Adaika, Y. Bekkar, S. Youmbai, L. Bourougaa, E. Lanez, M.L. Ben Amor, K. Nesba, T. Lanez, L. Bechki, *Appl Organomet Chem*, **2025**, 39,.
68. A. Yahiaoui, N. Benyza, A. Messai, T. Lanez, L. Elhafnaoui, **2024**, 8, 93–102.
69. M.L. BEN AMOR, E. LANEZ, Y. Bekkar, A. ADAIKA, T. LANEZ, K. NESBA, L. BECHKI, *ChemistrySelect*, **2025**, 10, 1–16.
70. L. Ozalp, S.S. Erdem, B. Yüce-Dursun, Ö. Mutlu, M. Özbil, *Comput Biol Chem*, **2018**, 77, 87–96.
71. J.J.P. Stewart, *J Mol Model*, **2009**, 15, 765–805.
72. S. Grimme, *Wiley Interdiscip Rev Comput Mol Sci*, **2011**, 1, 211–228.
73. D.S. Biovia, **2017**, 936, 240–249.
74. G. V Dhoke, C. Loderer, M.D. Davari, M. Ansorge-Schumacher, U. Schwaneberg, M. Bocola, *J Comput Aided Mol Des*, **2015**, 29, 1057–1069.
75. O. Trott, A.J. Olson, *J Comput Chem*, **2010**, 31, 455–461.
76. K.J. Bowers, E. Chow, H. Xu, R.O. Dror, M.P. Eastwood, B.A. Gregersen, J.L. Klepeis, I. Kolossvary, M.A. Moraes, F.D. Sacerdoti, in: Proceedings of the 2006 ACM/IEEE Conference on Supercomputing, 2006, pp. 84-es.

MOHAMMED LARBI BEN AMOR, ELHAFNAOUI LANEZ, YAHIA BEKKAR, AICHA ADAIKA,
TOUHAMI LANEZ, KAOUTHER NESBA, LAZHAR BECHKI

77. J.L. Banks, H.S. Beard, Y. Cao, A.E. Cho, W. Damm, R. Farid, A.K. Felts, T.A. Halgren, D.T. Mainz, J.R. Maple, *J Comput Chem*, **2005**, 26, 1752–1780.
78. A.Y. Toukmaji, J.A. Board Jr, *Comput Phys Commun*, **1996**, 95, 73–92.
79. J. Zielkiewicz, *J Chem Phys*, **2005**, 123,.
80. G.J. Martyna, M.L. Klein, M. Tuckerman, *J Chem Phys*, **1992**, 97, 2635–2643.